

## **5. PARAMETRIC SYSTEMS STUDIES**

**R. L. Miller, and R. A. Krakowski**

## CONTENTS

5.1. Introduction . . . . .	5-1
5.2. Models . . . . .	5-4
5.2.1. Plasma Physics Models . . . . .	5-4
5.2.2. Reactor Engineering Models . . . . .	5-9
5.2.3. Costing . . . . .	5-12
5.3. Parametric Results . . . . .	5-17
5.3.1. Sensitivity and Trade-Offs . . . . .	5-17
5.3.2. "Strawman" Design-Point Selection . . . . .	5-27
5.3.3. Alternative Configuration Options . . . . .	5-29
References . . . . .	5-38

## 5. PARAMETRIC SYSTEMS STUDIES

### 5.1. INTRODUCTION

A parametric systems analysis (PSA) computer code is used to identify "Strawman" TITAN design points and establish the context of the design by means of sensitivity and trade-off studies. The code was originally developed for use in the Los Alamos Compact Reversed Field Pinch Reactor (CRFPR) studies [1-3] and the cost database was updated in the course of the Los Alamos ATR/ST study [4]. Further possible updates of the cost database are discussed in Sec. 5.2.3. The PSA code is used as a centerpiece of a constellation of activities, characterized in Fig. 5.1.-1, that comprises the TITAN design activity.

The objective of the Systems Analysis Activity is the systematic study and determination of plant operating parameters through economic analysis and optimization of the power station. The Strawman designs are chosen to meet program design goals (e.g., minimal cost of electricity, COE, and high mass power density). Code models include steady-state surveys designed to assess sensitivities and trade-offs related to various TITAN operating configurations and assumptions, as well as time-dependent start-up/burn simulations (Sec. 4.5.2). These models are bench-marked and calibrated against more detailed plasma physics and magnetic models to provide a framework for the overall design process. At least as important as the Strawman designs themselves is the parametric context established by the trade studies.

As indicated on Fig. 5.1.-2, the PSA code identifies optimal parameters in a set of nested search loops centered on a convergence operation for the engineering Q-value,  $Q_E = 1/\epsilon$ , and the specified net-electric power,  $P_E$ , where  $\epsilon$  is the recirculating power fraction. For a given total coil thickness,  $\delta_c$ , this inner iteration searches for the value of  $Q_E$  that yields the specified  $P_E$  as the split between the toroidal-field coil (TFC) and poloidal-field coil (PFC) geometry varies, subject to the constraints of equal (but unspecified) coil current densities and the matching of fixed engineering and physics parameters. The PSA code algorithm used in the CRFPR study (Fig. 6.-1 of Ref. 3) has been modified to treat the equilibrium-field (EF) and ohmic-heating (OH) coil sets separately, allowing the consideration of superconducting EFCs. The total TF + OH coil thickness  $\delta_c$  that produces a minimum-COE design for an otherwise fixed geometry, including plasma minor radius, is first determined after convergence of the set  $(Q_E, P_{TH})$  for a given  $P_E$ . The outer-loop optimum is then

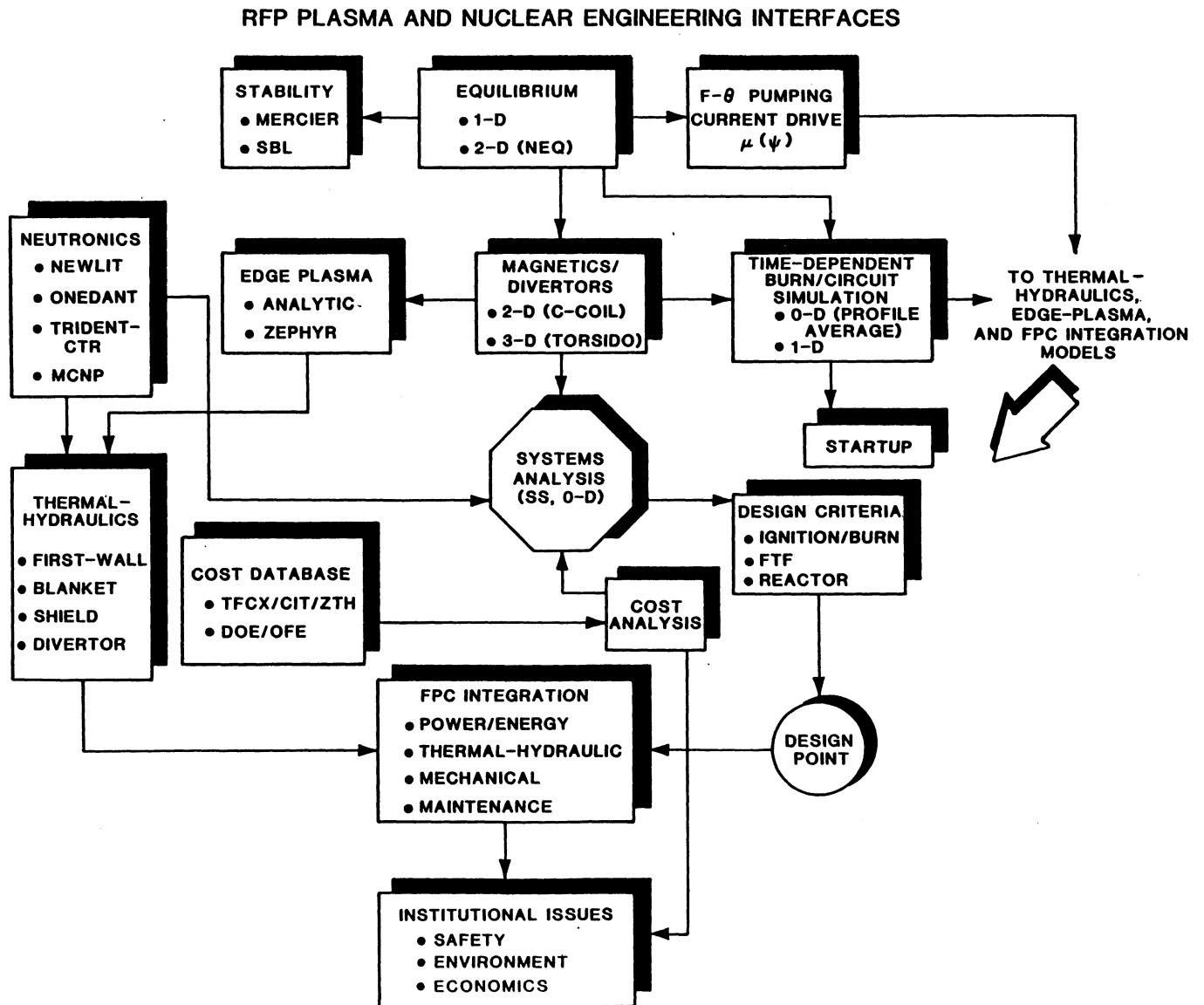


Fig. 5.1.-1. TITAN study approach organized by key plasma and nuclear engineering activities and interfaces. NEQ [5,6], NEWLIT [7], ONEDANT [8], TRIDENT-CTR [9], MCNP [10], CCOIL [2], TORSIDO [11], and ZEPHYR [12] are computer codes of potential use in the TITAN study.

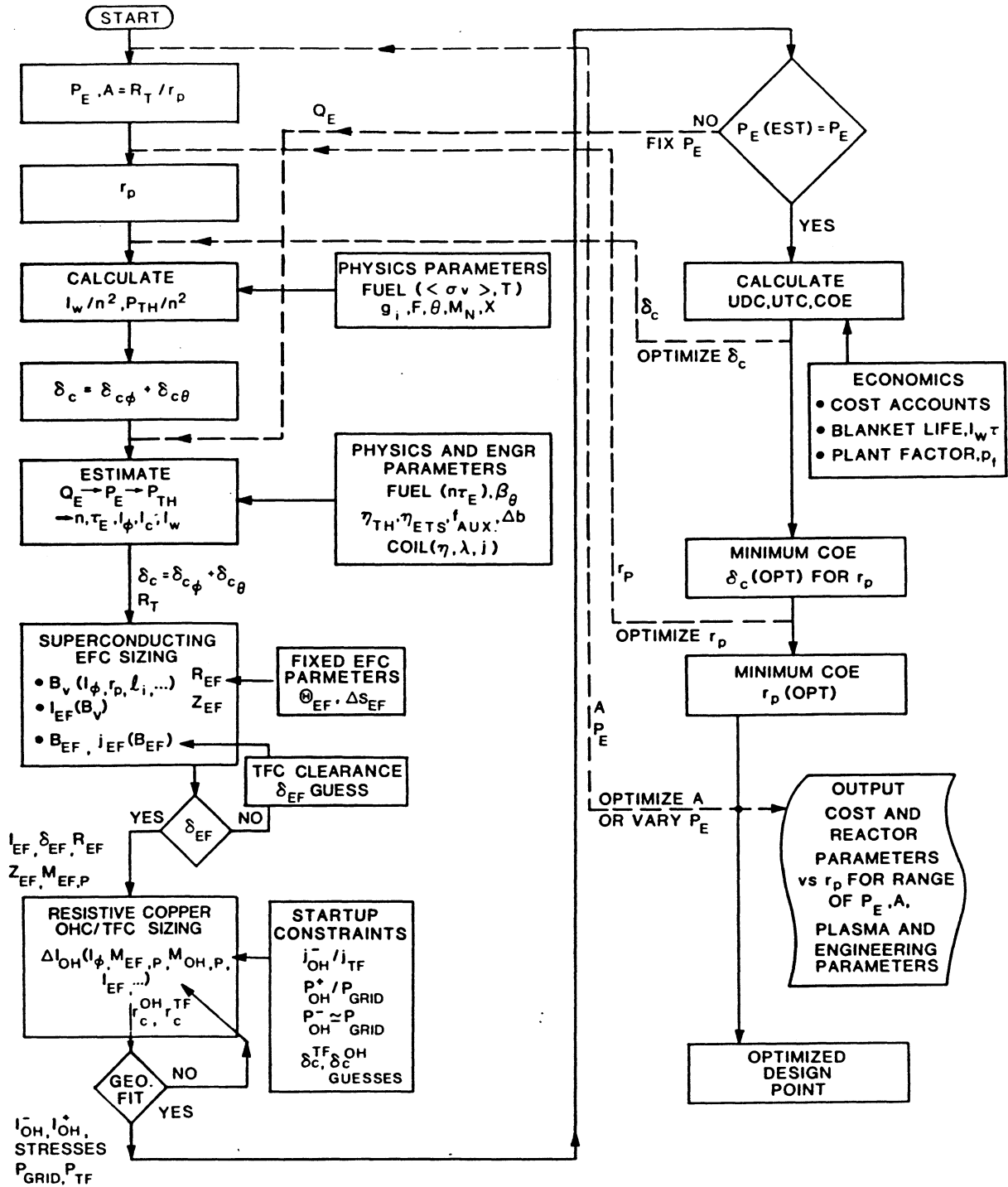


Fig. 5.1.-2. Parametric Systems Analysis (PSA) procedure used for the TITAN study, as adapted from CRFPR methods [1,2].

determined as a function of plasma radius,  $r_p$ , which shows a higher-order (lower) COE minimum. Generally,  $r_p$  is used as a display variable, with the respective minimum-COE design corresponding to a particular value of  $P_E$  and plasma aspect ratio,  $A = R_T/r_p$ . The outermost loop then varies the aspect ratio in search of an even lower minimum-COE system, although within realistic bounds, the optimum in  $A$  is relatively flat for the RFP. These fully-cost-optimized design points are then examined as a function of  $P_E$  and various physics, engineering, and economic parameters and options. The results of this analysis identify Strawman design points which serve as the starting points for conceptual engineering analysis and elaboration.

Section 5.2 summarizes the physics, engineering, and costing models used in the PSA code. Sec. 5.3 presents results of the PSA studies performed to date and summarizes the parameters of the present set of Strawman design points.

## 5.2. MODELS

### 5.2.1. Plasma Physics Models

The TITAN systems model begins with a steady-state, point-plasma model, corrected for profile effects. It is convenient to define a filling fraction  $x \equiv r_p/r_w$  for the circularized plasma in a toroidal chamber where  $r_w$  is the minor radius of the first wall. The parameter  $x$  is chosen to anticipate the first-wall geometry and scrape-off layer thickness in relating the volumetric fusion power to the average 14.1 MeV neutron first-wall loading.

The average plasma DT fusion (17.58 MeV/fusion) power density,  $P_F/V_p$ , is given by

$$P_F/V_p \text{ (W/m}^3\text{)} = 7.04 \times 10^{13} n_i^2 \langle \sigma v \rangle_{DT} g_{DT} . \quad (5.2.-1)$$

In the above equation,  $n_i$  is the average DT ion density,  $\langle \sigma v \rangle_{DT}$  is the DT fusion reactivity,  $g_{DT}$  is the fusion-power profile correction factor. The  $\langle \sigma v \rangle_{DT}(T)$  values used in this study are based on the recent Los Alamos experimental measurement and temperature-dependent fitting function [13] in the range  $0 < T < 20$  keV, with typical results summarized in Table 5.2.-I. Differences in physics assumption between the TITAN study and earlier CRFPR studies are summarized in Table 5.2.-II. For purposes of the TITAN study, a lower value of poloidal beta,  $\beta_\theta$ , and flatter radial profiles of plasma temperature and density

TABLE 5.2.-I  
MAXWELLIAN-AVERAGED DT FUSION CROSS SECTIONS [13]

T(keV)	$\langle\sigma v\rangle_{DT}(m^3/s)$	$\langle\sigma v\rangle_{DT}/T^2(m^3/s-keV^2)$
0.5	$5.58 \times 10^{29}$	$2.23 \times 10^{28}$
1.0	$6.71 \times 10^{27}$	$6.71 \times 10^{27}$
5.0	$1.33 \times 10^{23}$	$5.30 \times 10^{25}$
10.0	$1.12 \times 10^{22}$	$1.12 \times 10^{24}$
13.5	$2.21 \times 10^{22}$	$1.215 \times 10^{24}(\text{max})$
15.0	$2.71 \times 10^{22}$	$1.20 \times 10^{24}$
20.0	$4.29 \times 10^{22}$	$1.07 \times 10^{24}$
25.0(a)	$5.95 \times 10^{22}$	$9.52 \times 10^{25}$

(a) Out of nominal range of fitting function.

density have been assumed; the flatter profiles are a result of 1-D plasma simulations (Sec. 4.7.2.1). The "g" values reported in Table 5.2.-II measure the peaked-profile enhancement of fusion power (DT), ohmic heating (OHM), and Bremsstrahlung (BR) relative to the values obtained from flat profiles. Generally, the volume-averaged power density is given by

$$P_i \equiv \langle P_i(r) \rangle = \langle f_i[B(r), j(r), n(r), T(r)] \rangle, \quad (5.2.-2)$$

where the subscript "i" denotes fusion, radiation, or ohmic-heating power densities. The systems model calculates volume-averaged power densities,  $P_i$ , using average parameters; all profile information is contained in the profile enhancement factors  $g_i$ , where

$$P_i = g_i f_i(\langle B \rangle, \langle j \rangle, \langle n \rangle, \langle T \rangle). \quad (5.2.-3)$$

Henceforth, all quantities are volume-averaged except otherwise specified. The average current density, plasma density, and plasma temperature used in Eq. (5.2.-1) are defined as follows:

TABLE 5.2.-II  
COMPARISON OF BASELINE PHYSICS PARAMETERS

<u>Parameter</u>	<u>CRFPR [2-4]</u>	<u>TITAN(1-D)</u>
T(r)/T(0)	$J_0(\mu r)$	$1 - (r/r_p)^4$
n(r)/n(0)	$J_0(\mu r)$	$1 - (r/r_p)^{2.5}$
$\mu(r)/\mu(0)$	$\begin{cases} 1 & (r < r_r) \\ \frac{r_p - r}{r_p - r_r} & (r_r < r < r_p) \end{cases}$	$1 - (r/r_p)^8$
T(keV)	10.	10.
Poloidal beta, $\beta_\theta$	0.20	0.13
Pinch parameter, $\Theta$	1.55	1.47
Reversal parameter, F	-0.12	-0.11
Reactivity enhancement, $g_{DT}$	2.23	1.59
Ohmic heating, $g_{OHM}$	5.08	3.62
Bremsstrahlung, $g_{BR}$	1.52	1.33
$n\tau_E$ ( $m^3 s$ ) @ T = 20 keV	--	$1.1 \times 10^{20}$

$$j_\phi \equiv I_\phi / A_p , \quad (5.2.-4a)$$

$$n \equiv \frac{2\pi}{A_p} \int_0^{r_p} n(r) r dr , \quad (5.2.-4b)$$

$$T \equiv \frac{2\pi}{n A_p} \int_0^{r_p} T(r) n(r) r dr , \quad (5.2.-4c)$$

where  $I_\phi$  is the toroidal plasma current and  $A_p = \pi r_p^2$  is the plasma minor cross-sectional area. The profile factors are then defined as

$$g_i \equiv \frac{2\pi}{P_i A_p} \int_0^{r_p} P_i(r) r dr . \quad (5.2.-5)$$

The ohmic-heating profile correction factor, for example, becomes

$$g_{OHM} = \frac{2\pi \int_0^{r_p} \eta_{||} [n(r), T(r)] [j_{\phi}^2(r) + j_{\theta}^2(r)] r dr}{\eta_{||} (n, T) I_{\phi}^2 A_p} , \quad (5.2.-6)$$

where  $\eta_{||}$  is the classical Spitzer resistivity. It is the natural tendency for the RFP configuration to relax to a  $\beta = 0$ ,  $\mu \equiv \mu_0 \vec{j} \cdot \vec{B} / B^2 = \text{constant}$  (force-free) Taylor minimum-energy state [14], characterized by  $F$  (the reversal parameter),  $\Theta$  (the pinch parameter), and  $\mu(r)$ , where

$$F \equiv \bar{B}_{\phi}(r_p) / \langle B_{\phi} \rangle \quad (5.2.-7)$$

$$\Theta \equiv \bar{B}_{\theta}(r_p) / \langle B_{\phi} \rangle \quad (5.2.-8)$$

$$\mu(r) / \mu(0) \equiv \bar{j}(r) \cdot \bar{B}(r) / \bar{j}(0) \cdot \bar{B}(0) , \quad (5.2.-9)$$

again, with  $\bar{B}_{\phi}$ ,  $\bar{B}_{\theta}$ ,  $\bar{j}(r)$  being flux-surface-averaged quantities. Typically,  $\mu(r)$  is constant within the central plasma and decreases more-or-less linearly to zero near the cold plasma edge, where the highly resistive edge-plasma cannot support large current densities.

The plasma-surface-averaged poloidal magnetic field,  $\bar{B}_{\theta}(r_p)$ , is approximated by

$$\bar{B}_{\theta}(r_p) = \frac{\mu_0 I_{\phi}}{2\pi r_p} . \quad (5.2.-10)$$

The plasma self-inductance,  $L_p$ , is approximated by

$$L_p(H) = \mu_o R_T \left[ \ln \left( \frac{8R_T}{r_p} \right) + \frac{l_i}{2} - 2.0 \right], \quad (5.2.-11)$$

where  $l_i \equiv \langle B_\theta^2 \rangle / \bar{B}_\theta^2(a)$  is the plasma internal inductance per unit length normalized to  $\mu_o = 4\pi \times 10^{-7}$  H/m. The vertical field,  $B_V$ , required to maintain the plasma toroidal equilibrium becomes

$$B_V(T) = - \frac{\mu_o I_\phi}{4\pi R_T} \left[ \ln \left( \frac{8R_T}{r_p} \right) + \beta_\theta + \frac{l_i}{2} - \frac{3}{2} \right], \quad (5.2.-12)$$

Neglecting corrections for  $Z_{\text{eff}} > 1$ , the plasma pressure balance can be written in the form

$$I_\phi = \left[ \frac{2p}{\beta_\theta \mu_o} \right]^{1/2} 2\pi r_p, \quad (5.2.-13)$$

where the plasma pressure is  $p = 2nk_B T$  and  $k_B$  is the Boltzmann constant.

The PSA code searches for minimum-COE design points satisfying the ignition condition while balancing the plasma ohmic and fusion-product power inputs against radiation and transport losses, such that

$$P_\Omega + P_\alpha = P_{\text{RAD}} + P_{\text{TR}} \quad (5.2.-14)$$

at a profile-corrected Lawson parameter,  $n\tau_E$ , value consistent with the stipulated average plasma operating temperature,  $T$  [15]. The plasma ohmic power,  $P_\Omega$ , is given by

$$P_\Omega = g_{\text{OHM}} I_\phi^2 R_p = g_{\text{OHM}} \eta_{\parallel} j_\phi^2 V_p, \quad (5.2.-15)$$

where  $\eta_{\parallel}$  is the classical plasma resistivity. The plasma current is maintained at steady state by Oscillating Field Current Drive system (OFCD). The OFCD system power,  $P_{\text{CD}}$ , is (see Sec. 4.6)

$$P_{CD} = P_{\Omega} \left( 1 + \frac{Q_p}{Q_c} \right), \quad (5.2.-16)$$

where  $Q_p$  and  $Q_c$  characterize the plasma coupling and circuit performance, respectively.

The RFP energy confinement time,  $\tau_E$ , is assumed to scale from values obtained in present-day experiments according to

$$\tau_E(\text{PHYS}) = C_{\nu} [I_{\phi}(\text{MA})]^{\nu} r_p^2 f(\beta_{\theta}) \quad (5.2.-17)$$

with typical values of the scaling exponent,  $\nu$ , and numerical coefficient summarized in Table 5.2.-III. The function  $f(\beta_{\theta})$  models the soft-beta limit and assumed to have the form,  $f(\beta_{\theta}) = 1$  for  $\beta_{\theta} < \beta_{\theta c}$  ( $= 0.19$ ) and  $f(\beta_{\theta}) = (\beta_{\theta}/\beta_{\theta c})^8$  for  $\beta_{\theta} > \beta_{\theta c}$ . The energy confinement time of a PSA-code-determined minimum-COE design point,  $\tau_E(\text{OPT})$ , at  $P_E = 1,000$  MWe is typically consistent with  $\nu \approx 1.0$ . Smaller output reactors with smaller values of  $r_p$  typically require  $\nu > 1.0$  (i.e., better intrinsic energy confinement).

### 5.2.2. Reactor Engineering Models

Given a stipulated target net-electric power output,  $P_E$ , the thermal power output,  $P_{TH}$ , and recirculating power fraction,  $\varepsilon \equiv 1/Q_E$ , are determined for a nominal value of the thermal conversion efficiency,  $\eta_{TH}$ , such that  $P_E = \eta_{TH}(1 - \varepsilon)P_{TH}$ . The gross electrical power output is  $P_{ET} = \eta_{TH}P_{TH}$ . A

TABLE 5.2.-III

RFP ENERGY CONFINEMENT SCALING <sup>(a)</sup>	PARAMETERS
$\nu$	$C_{\nu}$
1.5	0.140
1.25	0.085
1.1	0.062
1.0	0.050
0.9	0.040

$$(a) \tau_E(s) = C_{\nu} [I_{\phi}(\text{MA})]^{\nu} r_p^2$$

fraction  $f_{\text{AUX}} = 0.07$  of  $P_{\text{ET}}$  is allocated for primary-loop pumping power and other auxiliary functions, such that  $P_{\text{AUX}} = f_{\text{AUX}}P_{\text{ET}}$ . The plasma ohmic-heating power,  $P_{\Omega}$ , resistive-coil Joule dissipation in the respective coil sets,  $P_{\text{TFC}}^{\Omega}$  and  $P_{\text{DFC}}^{\Omega}$ , and current-drive power,  $P_{\text{CD}}$ , complete the components of recirculating power for the TITAN. If the EFC is taken to be superconducting,  $P_{\text{EFC}}^{\Omega} = 0$ . Additionally, following the start-up transient, the OHC current can be slowly ramped down to zero, such that for purposes of the average steady-state power balance,  $P_{\text{OHC}}^{\Omega} = 0$ . The engineering Q-value figure of merit,  $Q_{\text{E}}$ , can be written as

$$Q_{\text{E}} = \frac{1}{\epsilon} = \frac{\eta_{\text{TH}}(M_{\text{N}}P_{\text{N}} + P_{\text{RAD}} + P_{\text{TR}} + P_{\Omega})}{P_{\Omega} + P_{\text{AUX}} + P_{\text{TFC}}^{\Omega} + P_{\text{DFC}}^{\Omega} + P_{\text{CD}}}, \quad (5.2.-18)$$

where  $M_{\text{N}}$  [assumed to be 1.33 pending calibration by neutronics calculations, (Sec. 8)] is the blanket fusion-neutron energy multiplication. The average neutron wall loading,  $I_{\text{w}}$ , is given by

$$I_{\text{w}}(\text{MW}/\text{m}^2) = \frac{P_{\text{TH}} x}{(2\pi)^2 A r_{\text{p}}^2 (M_{\text{N}} + 0.25)}, \quad (5.2.-19)$$

and  $x \equiv r_{\text{p}}/r_{\text{w}}$ . A scrape-off layer thickness of 0.05 m is presently assumed, such that  $r_{\text{w}} = r_{\text{p}} + 0.05$ .

The normal-conducting copper-coil resistivity is taken to be  $\rho_{\text{Cu}} = 2.0 \times 10^{-8} \Omega \text{ m}$ . Typically, the effective resistivity is increased by  $1/\lambda_{\text{c}}$ , where  $\lambda_{\text{c}} \approx 0.7$  is the assumed conductor filling fraction, pending a more-detailed design of the coil internals. The resistive coil density is consistent with a composition of 70 v/o copper conductor, 10 v/o stainless-steel structure, 10 v/o MgO insulation, and 10 v/o (drained) coolant. For superconducting EFCs, the maximum coil current density is

$$j_{\text{m}}(\text{MA}/\text{m}^2) = \frac{(96 - 6B_{\theta\text{c}})}{[1 + (B_{\theta\text{c}}/12)^{1.5}]}, \quad (5.2.-20)$$

where  $B_{\theta c}$  is the magnetic-field strength in Tesla, calculated at the EFC surface.

Drained blanket, shield, and coil masses are calculated using homogenized densities  $\rho = 7.75, 7.0, 7.3$  tonnes/m<sup>3</sup>, respectively. A PbLi eutectic breeder/coolant material density is 9.4 tonnes/m<sup>3</sup>, as used in the CRFPR [2,3] compared with 0.5 tonnes/m<sup>3</sup> for Li, one of the present TITAN options. The FPC mass,  $M_{FPC}$ , is used to compute mass utilization  $M_{FPC}/P_{TH}$  (tonne/MWt) and mass power density, MPD (kWe/tonne), figures of merit (Ref. 16 and Appendix C of Ref. 4).

Steady-state operation of the TITAN RFP reactor relieves thermal-fatigue problems and increases the system reliability. Commercial operation also requires adequate maintenance access. The goal of incorporating fully remote, single-piece maintenance in the reactor building and hot cell exerts another strong influence on system economics, particularly from the viewpoint of plant availability. Remote handling is presently undergoing rapid development, and it is assumed that the necessary equipment will have been developed.

System redundancy, steady-state operation, ease of reactor torus replacement, and development of reliable components should permit the nominal overall plant availability of 76% for the TITAN designs. Steady-state operation should considerably improve reliability for the application of economically optimum engineering safety factors. The plant availability is reduced from 100% because of outage time for scheduled,  $t_s$ , and unscheduled,  $t_u$ , maintenance periods. The plant availability,  $p_f = (365 - t_u - t_s)/365$ , where  $t_u$  and  $t_s$  are expressed in days. The scheduled outage time has been estimated as 28 days per reactor-torus replacement. To achieve the target availability of 76%, the unscheduled outage is set at 60 days per year. The periodic first-wall and blanket replacement becomes an important operational feature. A first-wall lifetime of  $I_w \tau = 15$  MWyr/m<sup>2</sup> is assumed, which, together with a plant availability of 76% results in annual FW/B/S replacement at  $I_w \approx 20$  MW/m<sup>2</sup>. Higher wall loadings require additional increments of 28 days of replacement, resulting in higher values of the COE which in turn determines the minimum of the COE as a function of the wall loading.

An alternative availability algorithm has been proposed by the FEDC group, based on empirical coal and fission experience as it relates to plant size and penalizing for higher wall-loading according to

$$p_f^* = 0.827 - 0.060 \left( \frac{P_E(\text{MWe})}{1000} \right) - 0.017 \left( \frac{I_w(\text{MW/m}^2)}{20} \right) . \quad (5.2.-21)$$

For the nominal min-COE Strawman design point,  $p_f^* \approx p_f \approx 0.75$ , but the cost penalty of lower-wall-loading operation is reduced using this algorithm.

### 5.2.3. Costing

The Cost of Electricity (COE) is the most important evaluation tool to optimize and to compare with alternative energy sources. Both constant-1986 and then-current-1991 dollar analyses are used to evaluate the TITAN economic parameters for an assumed 5-yr construction time. The general equation for bus-bar energy cost is given by

$$\text{COE} = \frac{C_{AC} + (C_{O\&M} + C_{SCR} + C_F)(1 + E)^P}{8760 P_E p_f} , \quad (5.2.-22)$$

where

- COE = Cost of electricity in constant or then-current dollars (mills/kWeh),
- $C_{AC}$  = Annual capital cost charge, equals total capital cost multiplied by fixed charge rate (0.10 for constant-dollar analysis or 0.15 for then-current-dollar analysis),
- $C_{O\&M}$  = Annual operations and maintenance cost,  $C_{40} + C_{41} + \dots + C_{47}$ ,
- $C_{SCR}$  = Annual scheduled component replacement cost,  $C_{50} + C_{51}$ ,
- $C_F$  = Annual fuel costs,  $C_{02}$  and  $C_{03}$ ,
- E = Escalation rate equals 0.0 for constant-dollar analysis and 0.05 for then-current-dollar analysis,
- P = Construction period (yr),
- $P_E$  = Net plant capacity (MWe), and
- $p_f$  = Plant availability factor.

The essential elements of the TITAN cost database [2,4] are summarized in Table 5.2.-IV. Costs as scaled from 1980 to 1986 using the factor 1.348 [4]. For purposes of costing in the parametric systems model, the reactor building is divided into a variable-volume reactor cell, housing the FPC and vacuum tank, and a fixed-volume region, housing the primary heat-transfer/transport loops. The volume of the latter portion is estimated to be  $1.55 \times 10^5 \text{ m}^3$  and is similar to that of the STARFIRE design [17]. The reactor room is modeled by a rectilinear enclosure extending horizontally 9 m beyond the FPC with a height approximately six times that of the FPC, such that  $V_{RB} = - [2(R_T + r_s + 9)]^2 (12r_s) \text{ m}^3$ . The basic building structure (Account 21.2.1) is priced at  $300 \text{ \$/m}^3$ , a value intermediate between that of STARFIRE [17] and MARS [18], to which is added 2 M\$ for building services (Account 21.2.2), 30 M\$ for containment structures (Account 21.2.3), and 7.5 M\$ for architectural costs (Account 21.2.4).

The Main Heat Transfer System includes a liquid-metal (LM) loop serving the blanket, divertor, and shield. Allowances are made for a fraction,  $f_w$ , of thermal power to be delivered to a pressurized-water loop. The cost of the LM loop (Account 22.2.1) is estimated to be  $3.40 \times 10^4 P_{TH} (1 - f_w) \text{ M\$}$  and that of a pressurized-water loop (Account 22.2.3) is estimated to be  $3.50 \times 10^4 P_{TH} f_w \text{ M\$}$ , these estimates being calibrated by the dual-media (PbLi + H<sub>2</sub>O) MARS design [18] with a reduction of 80% of the dominant piping costs of that design to reflect the shorter pipe runs in the TITAN case. This model results in a  $\sim 50 \text{ M\$}$  increase in cost over the pressurized-water Main Heat Transfer System in STARFIRE [17]. In the TITAN case, where Li is the sole primary coolant,  $f_w = 0$ , unlike the dual-media system of the CRFPR. The LM inventory in the system consists of 95% of the blanket volume, corrected by a factor of 1.09 to account for the FPC ducts connecting the blanket through the TFC/PFC sets to the main manifolds. To this variable volume is added a fixed increment ( $\sim 500 \text{ m}^3$ ) for the primary-loop inventory, a value assumed to be relatively constant over the parameter range of interest. The cost of the primary-loop LM is reported under Special Materials (Account 26), insofar as it is salvageable and reuseable. The unit cost of the LM (PbLi or Li) is an increasing function of the <sup>6</sup>Li enrichment,  $f_{6Li}$ .

The first-wall/blanket/divertor (or limiter) replacement cost estimate applies a factor of two to the direct cost of these components to allow for the handling/replacement of the spent reactor torus. For an assumed first wall life of  $I_w \tau = 15 \text{ MWyr/m}^2$  at a cost-optimized neutron wall loading,  $I_w \approx 20 \text{ MW/m}^2$  and

TABLE 5.2.-IV  
SUMMARY FUSION REACTOR COST DATABASE<sup>(a)</sup>

<u>ACC. NO</u>	<u>ACCOUNT TITLE</u>	<u>(M\$, 1980)</u>
20.	Land and land rights	3.3
21.	Structures and site facilities	
21.1	Site improvements and facilities	11.15
21.2	Reactor building	$3. \times 10^{-4} V_{RB} + 39.5$
21.3	Turbine building	33.5
21.4	Cooling structures	$7.135(P_{ET}/1000)^{0.3}$
21.5	Power supply and energy storage	9.16
21.6	Miscellaneous buildings	76.5
21.7	Ventilation stack	1.81
21.98	Spare parts (2%)	
21.99	Contingency (15%)	
22.	Reactor Plant Equipment	
22.1	Reactor Equipment	
22.1.1	Blanket and first-wall structure	$0.0533 M_{BL}$
22.1.2	Shield	$0.015 M_{SHD}$
22.1.3	Magnet coils	$0.040 M_C(NC)$ or $0.080 M_C(SC)$
22.1.4	Supplemental heating systems	$1.65 P_{rf}$
22.1.5	Primary structure and support	$0.1125 V_{STR}$
22.1.6	Reactor vacuum system	$0.015 M_{VAC} + 0.83(P_F/250)$
22.1.7	Power supply (switching & energy storage)	$1.0 + 0.0148(P_C^Q + P_{CD})$
22.1.8	Impurity control system	$0.0026 V_{VAC}$
22.1.9	Direct energy conversion	0.0
22.1.10	ECRH Breakdown system	2.82
22.2	Main heat transfer system	
22.2.1	Primary coolant (LM)	$0.034 P_{TH} (1 - f_w)$
22.2.2	Intermediate coolant system	0.0
22.2.3	FW/Limiter/Shield coolant system (H <sub>2</sub> O)	$0.035 P_{TH} f_w$

TABLE 5.2.-IV (Cont.)  
SUMMARY FUSION REACTOR COST DATABASE<sup>(a)</sup>

<u>ACC. NO</u>	<u>ACCOUNT TITLE</u>	<u>(M\$, 1980)</u>
22.3	Auxiliary cooling systems	$6.7 \times 10^4 P_{TH}$
22.4	Radioactive waste treatment	$1.2 \times 10^3 P_{TH}$
22.5	Fuel handling and storage	$9.65 \times 10^3 P_{TH}$
22.6	Other reactor plant equipment	$1.09 \times 10^2 P_{TH}$
22.7	Instrumentation and control	23.41
22.98	Spare parts allowance (2%)	
22.99	Contingency allowance (15%)	
23.	Turbine plant equipment	
23.1	Turbine-generators	$59.9 (P_{ET}/1000)^{0.7}$
23.2	Main steam system	$4.80(P_{TH}/2860)$
23.3	Heat rejection systems	$33.0 (P_{TH}/2860)^{0.8}$
23.4	Condensing system	$13.8 (P_{ET}/1000)^{0.9}$
23.5	Feed heating system	$7.55(P_{TH}/2860)$
23.6	Other turbine plant equipment	$40.9 (P_{ET}/1000)^{0.6}$
23.7	Instrumentation and control	$7.80(P_{ET}/1000)^{0.3}$
23.98	Spare parts allowance (2%)	
23.99	Contingency allowance (15%)	
24.	Electric plant equipment	
24.1	Switchgear	$8.6 (P_{ET}/1000)$
24.2	Station service equipment	$14.2 (P_{ET}/1000)$
24.3	Switchboards	$5.4 (P_{ET}/1000)$
24.4	Protective equipment	2.11
24.5	Electrical structures and wiring containers	$11.12 + 6.28(P_{ET}/1440)$
24.6	Power and control wiring	$23.0 + 13.0(P_{ET}/1440)$
24.7	Electrical lighting	8.2
24.98	Spare parts allowance (4%)	
24.99	Contingency allowance (15%)	

TABLE 5.2.-IV (Cont.)  
SUMMARY FUSION REACTOR COST DATABASE<sup>(a)</sup>

<u>ACC. NO</u>	<u>ACCOUNT TITLE</u>	<u>(M\$, 1980)</u>
25.	Miscellaneous plant equipment	
25.1	Transportation and lifting equipment	15.68
25.2	Air and water service systems	12.35
25.3	Communications equipment	6.22
25.4	Furnishings and fixtures	1.20
25.98	Spare parts allowance (3%)	
25.99	Contingency allowance (15%)	
26.	Special Materials	
26.1	Reactor LM coolant/breeder <sup>(b)</sup>	PbLi: $M_{LM}(7.83f_6Li + 2.46)10^{-3}$ Li: $M_{LM}(1169f_6Li - 58.0)10^{-3}$
26.4	Other	0.25
90.	Total direct cost (TDC)	
91.	Construction facilities, equipment, and services (10%)	
92.	Engineering and construction management services (8%)	
93.	Other costs (5%)	
94.	Interest during construction, (IDC, 10%/yr)	
95.	Escalation during construction, (EDC, 5%/yr)	
99.	Total cost	

(a) Gross electric,  $P_{ET}$ , net electric,  $P_E$ , and total thermal,  $P_{TH}$ , powers given in MW. Volumetric  $V(m^3)$  abbreviations or corresponding mass  $M(\text{tonne})$  costs for the fusion power core (FPC) and related items are given as follows:

$$\text{Reactor building, } V_{RB} = 4(R_T + r_S)^2(12r_S) + 1.55 \times 10^5 \text{ (m}^3\text{)}$$

$$\text{Blanket structure (5\%), } M_{BL}(\text{tonne}), \text{ Shield, } M_{SHD}(\text{tonne})$$

$$\text{Magnet coils, } M_C(\text{tonne}), \text{ Structure, } V_{STR}(\text{m}^3)$$

$$\text{Vacuum tank, } M_{VAC} = (0.07)(7.8)2\pi[(R_T + r_S + 3)^2 + 4r_S(R + r_S + 3)] \text{ (tonne)}$$

(b) Liquid-metal,  $M_{LM}$  (tonne):  ${}^6\text{Li}$  enriched,  $0.075 < f_6Li < 0.90$ .

a plant factor  $\approx 0.76$ , routine replacement occurs annually. Account 50 represents  $\sim 3\%$  of the base-case COE for the TITAN and is distinct from the nominal annual O&M charge (Accounts 40-47, 51), conservatively estimated [19-20] to be 2% of the direct cost. This scheme costs the first reactor, first wall, and blanket twice, and credit for any reactor-torus component reuse (i.e., TFCs or shield) is not taken.

An updating of the prevailing cost accounting scheme [19-20] and unit-cost database is presently underway [21-22], subject to community review and consensus. Cost values obtained under the revised scheme are not expected to differ dramatically from the results reported herein. A preliminary comparison showed overall agreement of the direct-cost models to within 5%.

### 5.3. PARAMETRIC RESULTS

#### 5.3.1. Sensitivity and Trade-Offs

The CRFPR framework studies [2,3,23,24] focused on a design with a neutron wall loading of  $I_w \approx 20 \text{ MW/m}^2$  [CRFPR(20)], high-coverage (poloidal) pump limiters, a self-cooled  $\text{Pb}_{83}\text{Li}_{17}$ /ferritic-steel (HT-9) blanket, thin (0.10-m) steel shielding, closely coupled copper-alloy toroidal-field (TFCs) and poloidal-field coils (PFCs, includes both ohmic-heating, OHCs, and equilibrium-field coils EFCs), oscillating-field current drive (OFCD) for steady-state operation [25-26], and single-piece FPC (800-tonne PFC, 300-tonne first-wall/blanket/shield/TFC) maintenance.

The present focus of the TITAN study is a divertor-based [27], high-neutron-wall-loading ( $10\text{-}20 \text{ MW/m}^2$ ) design that also invokes OFCD for steady-state operation, retaining the motivation of high power density, compact fusion [28-30]. A range of pool- and loop-type blanket concepts is being considered. The desire to eliminate steady-state power consumption in the resistive EFC (53.5 MW for the CRFPR(20) framework design [22-23]) combined with a desire for a more open FPC geometry, which in turn is penalized by poorer coupling of PFCs to the plasma, points towards cost and operational incentives for otherwise more expensive superconducting EFCs, particularly if pool-type blankets, resistive-coil divertors, and more conservative physics assumptions (lower beta, flatter plasma profiles) are used. The OHCs and TFCs in TITAN, however, have remained as resistive-coil systems in order to retain a compact reactor torus, with the OHC being used and sized for start-up conditions only. Both OHCs and TFCs ideally would also serve current-drive functions, depending on the electrical

design of the intervening first wall, blanket, and shield. The OHC is also sized for full grid power applied in the back-biased condition and 20% of grid power available for resistive OHC losses in the forward-bias condition just prior to application of OFCD and steady-state operation. Somewhat higher plasma currents are required compared to the CRFPR(20) design because, for purposes of this section, the maximum poloidal beta has been decreased from  $\beta_{\theta} = 0.2$  to a more conservative value of 0.13, and flatter density and temperature profiles have been assumed, as suggested by one-dimensional plasma simulations performed as part of the TITAN study (see Sec. 4.7.2.1).

In order to examine at the earliest stages of the TITAN study the impact and sensitivities of the above-described changes, the systems model described in Ref. 3 was expanded to include a self-consistent treatment of separate OHCs and EFCs, as depicted in Fig. 5.3.-1. The scaling of poloidally symmetric toroidal-field divertors [27] and OFCD [2,25,26] was also included in the optimization algorithm. The computational algorithm used remains essentially as described in Ref. 3. As for any model of this nature, best choices for input are made on the basis of separate and detailed neutronics, plasma equilibrium, OFCD, divertor, and thermal-hydraulic calculations; important tradeoffs like construction time versus size and complexity, mean-time-to-repair versus mean-time-to-fail as a function of power density and size, and elasticity of nuclear and size economies of scale for key components remain inadequately resolved, however, and in need of future work.

Table 5.3.-I lists key design variables that were either fixed or varied in the re-optimization of the RFP reactor for the TITAN study. The blanket/shield standoff distance between the first wall and TFC/OHC sets is typical of a self-cooled,  ${}^6\text{Li}$ -enriched liquid-metal blanket, although a range of pool and loop concepts is being examined. The range of thermal-conversion efficiencies considered reflects primarily the blanket choice and whether or not the first wall and/or divertor chamber walls require a separate and possibly lower-temperature coolant.

The variation of cost with plasma aspect ratio,  $A = R_T/r_p$ , is weak in the range examined ( $A = 5-9$ ). Establishing a maximum grid power of  $P_{\text{GRID}} \approx 300$  MWe delivered to the OHC in the back-bias mode during start-up, and maintaining the peak von Mises stresses in the OHC below  $\sim 200$  MPa sets a limit of  $A \geq 5.5-6$ ; a baseline value of  $A = 6.5$  was selected to allow for added start-up flux. Figure 5.3.-2 gives the last level of constant-1986 COE minimization (i.e.,  $r_p$  variation) for the baseline ( $A = 6.5$ ); the effects of normal-conducting (NC)



TABLE 5.3.-I  
 FIXED AND VARIED PARAMETERS FOR TITAN RFP REACTOR  
 OPTIMIZATION AND SENSITIVITY STUDIES<sup>(a)</sup>

Minor plasma radius, $r_p$ (m)	[0.60]
Plasma aspect ratio, $A = R_T/r_p$	[6.5]
Plasma average temperature, T(keV)	10.
Poloidal $\beta_\theta$	[0.13]
Temperature/density profiles, $T(r)/T(0)$ , $n(r)/n(0) = 1 - (r/r_p)^\nu$ $\nu = 4, 2.5$	
Lawson parameter, $n\tau_E(10^{20} \text{ s/m}^3)$	1.60
Pinch parameter, $\Theta = B_\theta(r_p)/\langle B_\phi \rangle$	1.47
Reversal parameter, $F = B_\phi(r_p)/\langle B_\phi \rangle$	-0.11
Thermal-conversion efficiency, $\eta_{TH}$	[0.40]
EFC option	SC or NC
OHC, TFC, or DFC options	NC
Blanket/gap/shield standoff, $\Delta(m) = \Delta b + \Delta g + \Delta s$	[0.78]
EFC shield standoff	[0.0(NC), 1.5(SC)]
Blanket multiplication, $M_N$	1.33
SC coil current density, $j_c(\text{MA/m}^2)$ <sup>(b)</sup>	$(96.-6B_{\theta c})/[1 + (B_{\theta c}/12)^{1.5}]$
NC current density, $j_c(\text{MA/m}^2)$ <sup>(c)</sup>	$\leq 50.$
Plant factor, $p_f$	(28 day/FPC scheduled maintenance, 60 day/year unscheduled maintenance)
FPC radiation lifetime, $I_w\tau(\text{MWyr/m}^2)$	[15.]
Typical FPC unit costs (\$/kg, 1986)	
♦ First-wall/blanket	
- $\text{Pb}_{83}\text{Li}_{17}(90\% \text{ } ^6\text{Li})$	12.8
- HT-9	53.9
♦ Shield	20.2
♦ NC coil	53.9
♦ SC coil	107.8
♦ Structure	20.2
♦ OFCD power costs (\$/kVA)	[20.0]
OFCD plasma/circuit Q-values	[100]/[100.]

(a) Values in brackets [] were varied, with nominal design value being shown.

(b) Ref. 16.

(c) Cost optimization usually set  $j_c$  for resistive coils far below this limit, with  $j_c = 5-10 \text{ MA/m}^2$  being typical.

versus superconducting (SC) EFCs and the net electric power variations are shown. The secondary results of  $I_w$  (MW/m<sup>2</sup>) and FPC mass power density, MPD (kWe/tonne), are also shown. Comparison of generally common-basis costs are made with the STARFIRE [17], MARS [18], and the Spherical Torus Advanced Tokamak Reactor [4] (ATR/ST, a low-aspect-ratio extrapolation of the present tokamak database, and also a system with SC/EFC, NC/TFC, and OFCD, but using RF start-up and no OHC).

The most prominent feature of Fig. 5.3.-2 is the shallowness of the COE versus  $r_p$  (and hence,  $I_w$ ) minimum, although the compressed COE scale should be noted. Nevertheless, increasing  $I_w$  from 5 to 10 and then to the COE-minimum of 20 MW/m<sup>2</sup> results only in a 3 and 11% reduction, respectively, in COE. Other developmental and operational (i.e., single-piece maintenance) incentives not included in the present costing model can justify the higher- $I_w$ , high-MPD design points that reside closer to the COE minimum. The dependence of COE on net plant capacity shown on Fig. 5.3.-2 is typical of the nuclear economy of scale and is shown explicitly on Fig. 5.3.-3; a comparison with fission and fossil (coal) energy costs [34,35] is also given.

An interim TITAN baseline reactor has been chosen to explore further technology requirements and cost sensitivities. Typical physics, engineering, and costing parameters are listed on Table 5.3.-II. This system is based on superconducting EFCs and generates a net electric power of  $P_E = 1,000$  MWe(net).

The sensitivity of COE for the  $I_w \approx 19$  MW/m<sup>2</sup> baseline design to changes in  $P_E$ , EFC choice,  $I_w$ , MPD, and other key design parameters is shown in Fig. 5.3.-4. Both  $I_w \approx 19$  MW/m<sup>2</sup> and MPD = 544 kWe/tonne appear to be optimum values. Changes in the baseline values for beta ( $\beta_0 = 0.13$ ) and FPC lifetime ( $I_w \tau = 15$  MW/m<sup>2</sup>) by more than ~ 25% and ~ 50%, respectively, are required before more than a 10% respectively, effect is observed on COE. This relative insensitivity is a result of the small percentage contributed by the FPC to the overall plant direct cost (~ 7% compared to 25-30% for STARFIRE [17] and MARS [18]), despite higher unit (\$/kg) costs assumed for the TITAN reactor. It should be noted that these COE sensitivities represent single-point variations, and the resulting minimum-cost designs reflect a number of simultaneously changing features; for instance, the decrease in FPC radiation life increases cost both because of increased operating (blanket/shield replacement) cost as well as decreased  $I_w$  and MPD, with the latter decreased power density and increased direct costs resulting from the system re-optimization to maintain an

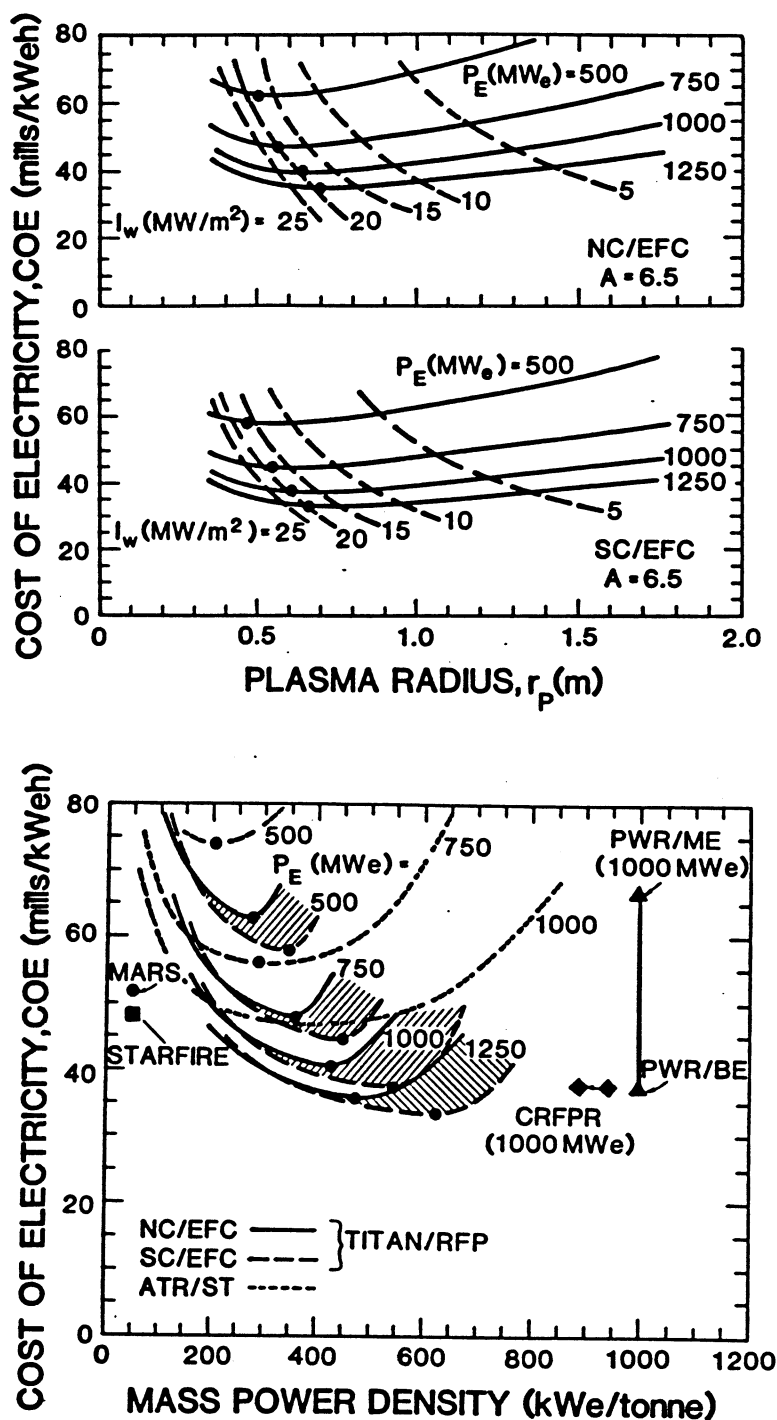


Fig. 5.3.-2. Dependence of near-minimum-COE designs on plasma minor radius,  $r_p$ , net electric power,  $P_E$  (MWe), and superconducting versus normal-conducting EFC options. Shown also is the secondary dependence of neutron wall loading,  $I_w$  (MW/m<sup>2</sup>), and mass power density, MPD (kWe/tonne); comparison with CRFPR(20) [3], STARFIRE [17], MARS [18], the Advanced Tokamak Reactor based on the Spherical Torus, ATR/ST [4,32], and a typical PWR [33], are also shown.

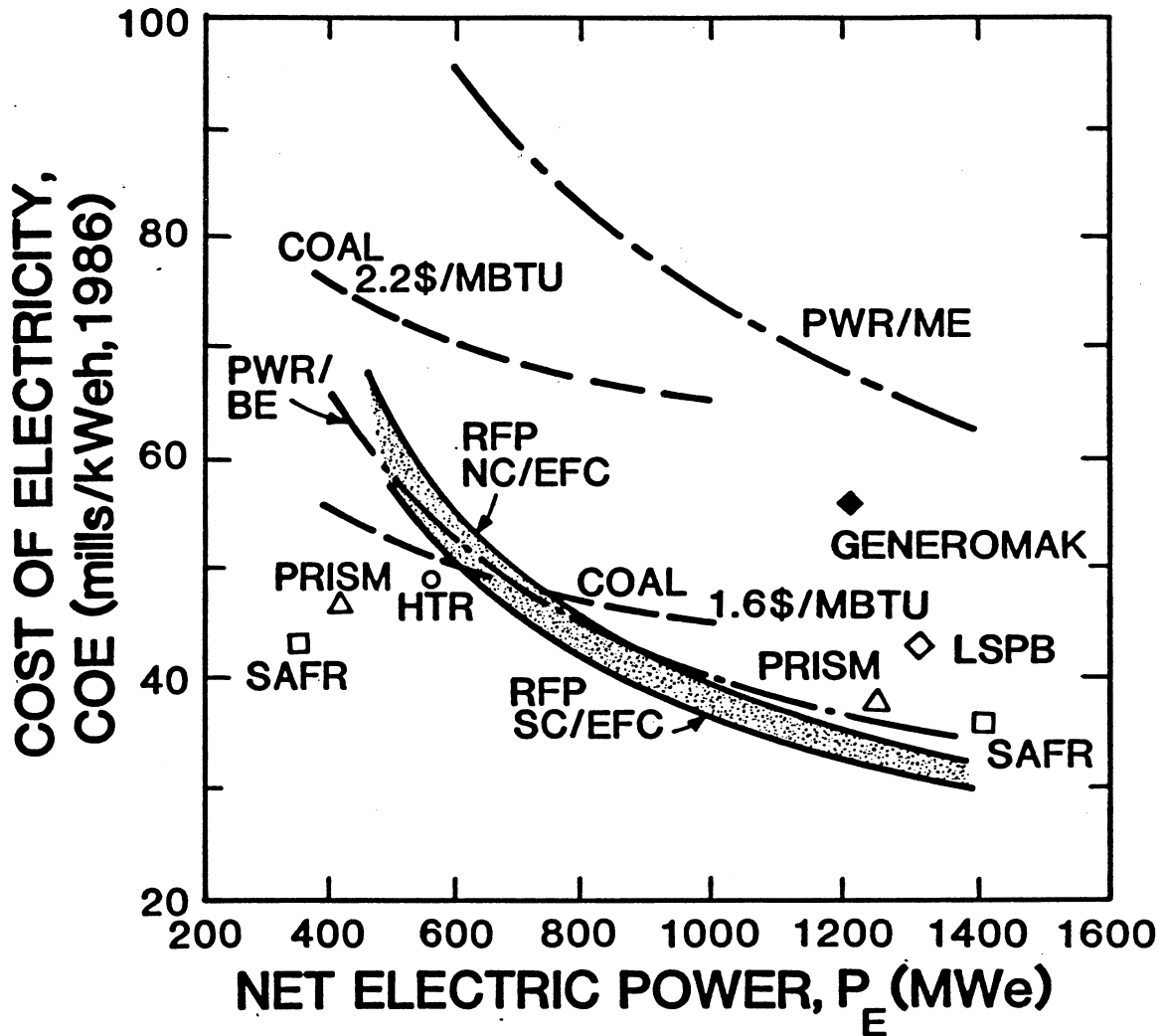


Fig. 5.3.-3. Projected cost of electricity, COE, as a function of net plant capacity and a comparison with fossil and fission costs for a range of coal costs (oil at 10 \$/bbl equals  $\sim 2.0$  \$/MBTU), medium-experience and best-experience PWR fission reactor costs (respectively, PWR/ME and PWR/BE). The GENEROMAK [16] and "new-age" inherently-safe fission reactor cost projections [34] are also shown (LSPB: Large Scale Prototype Breeder, SAFR: Sodium Advanced Fast Reactor, PRISM: Power Reactor Inherently Safe, and HTR: High Temperature gas-cooled Reactor).

TABLE 5.3.-II

## SUMMARY OF 1000-MWe(net) BASELINE RFP DESIGN

<u>Plasma Parameters</u>	
Minor plasma radius, $r_p$ (m)	0.61
Major plasma radius, $R_T$ (m)	3.96
Plasma current, $I_\phi$ (MA)	21.7
Plasma density, $n(10^{20}/m^3)$	8.17
Poloidal field at plasma surface, $B_\theta$ (T)	7.11
Fusion power density, $P_F/V_p$ (MW/m <sup>3</sup> )	83.2
Plasma ohmic dissipation, $P_\Omega$ (MW)	32.8
<u>Poloidal-Field Quantities</u>	
Coil thickness, $\delta_{c\theta}$ (m)	0.30
Average minor radius, $r_{c\theta}$ (m)	1.62
Coil field, $B_{c\theta}$ (T)	1.69
OHC current density, $j_{c\theta}$ (MA/m <sup>2</sup> )(b)	18.0
Mass of OHC set, $M_{OHC}$ (tonne)	396.9
EFC current density, $j_{c\theta}$ (MA/m <sup>2</sup> )(c)	18.0
Mass of EFC set (tonne)	376.8
OHC dissipation during back-bias (MW)	370.6
<u>Toroidal-Field Quantities</u>	
Coil thickness, $\delta_{c\phi}$ (m)	0.04
Average minor radius of coil, $r_{c\phi}$ (m)	1.45
Mass of coil, $M_{TFC}$ (tonne)	39.1
TFC current density, $j_{c\phi}$ (MA/m <sup>2</sup> )	18.0
Ohmic dissipation during burn, $P_\Omega^{TFC}$ (MW)	49.4
Mass of divertor coil, $M_{DFC}$ (tonne)	5.3
Ohmic dissipation in divertor, $P_\Omega^{DFC}$ (MW)	33.0

TABLE 5.3.-II (Cont.)  
SUMMARY OF 1000-MWe(net) BASELINE RFP DESIGN

<u>Engineering Summary</u>	
Engineering Q-value, $Q_E = 1/\epsilon$	5.27
Fusion power, $P_F$ (MW)	2,416
Total thermal power, $P_{TH}$ (MW)	3,086
Neutron Wall Loading, $I_w$ (MW/m <sup>2</sup> )	19.0
First-wall major radius, $r_w$ (m)	0.66
Masses (tonne)	
♦ first wall/blanket	40.6
♦ shield	972.8
♦ total coil set	818.1
♦ FPC mass	1,836.8
♦ FPC structure	1,052.7
System power density, $P_{TH}/V_{FPC}$ (MWt/m <sup>3</sup> )	12.6
Mass power density, $1,000P_E/M_{FPC} = MPD$ (kWe/tonne) <sup>(d)</sup>	545.
<u>Cost Summary</u>	
Cost of electricity, COE(mills/kWeh)	37.2
Unit direct cost, UDC(\$/kWe)	1,488.
Total cost, TC(M\$)	2,027.
FPC unit cost (\$/kg) <sup>(e)</sup>	53.0
Fractions of total directed TDC	
♦ reactor plant equipment, RPE/TDC	0.37
♦ fusion power core cost, FPC/TDC <sup>(d)</sup>	0.0655

(a) All designs are for baseline parameters given in Table 5.3.-I,  
 $A = R_T/r_p = 6.5$ ,  $\beta_\theta = 0.13$ .

(b) Peak current in back-biased state, decreases by factor of ~ 2 in forward-bias state, subsequently decays to zero upon initiation of OFCD.

(c) Superconducting magnet.

(d) Does not include structure.

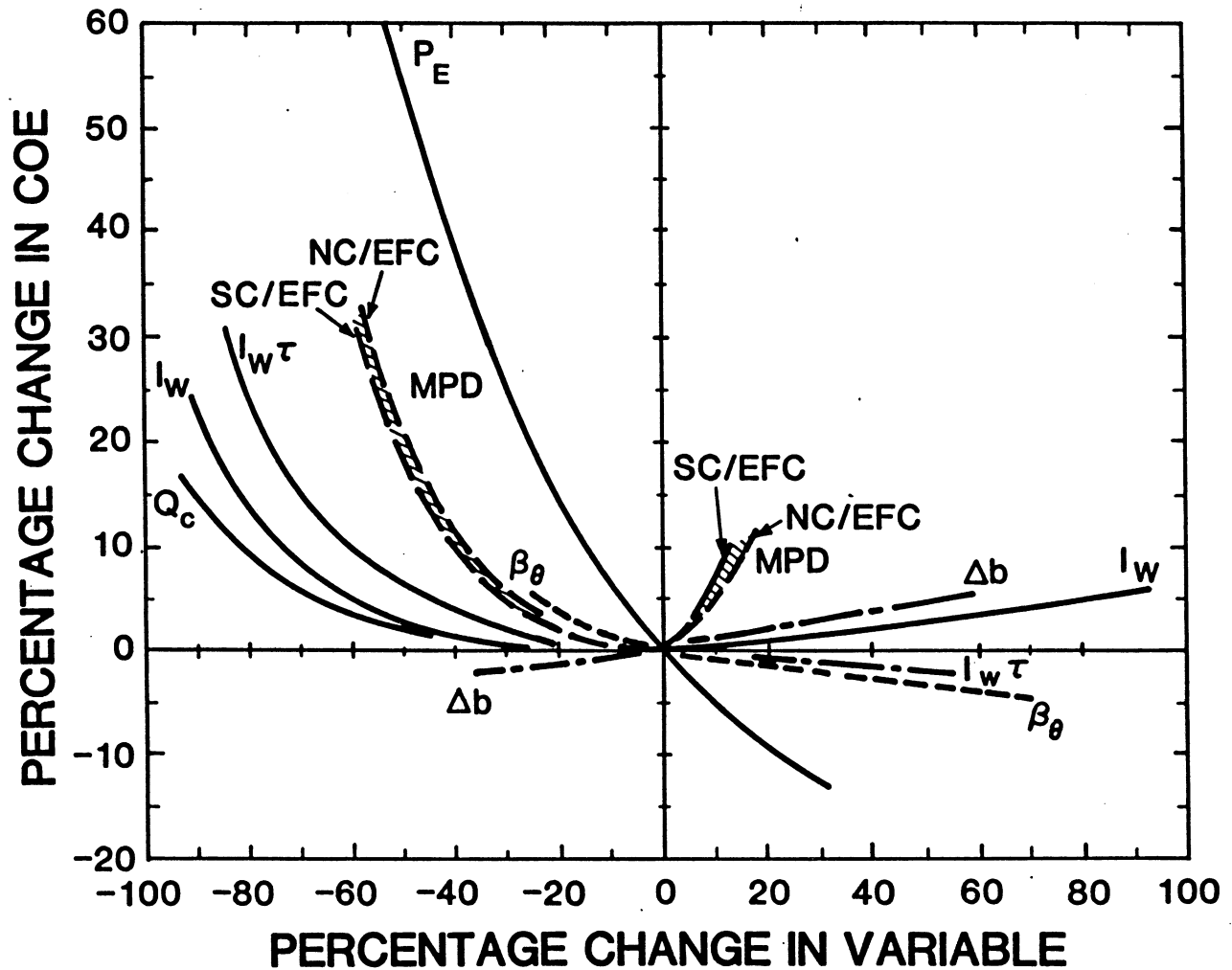


Fig. 5.3.-4. Sensitivity of COE to perturbations in key physics and engineering characteristics of the  $I_w \approx 19 \text{ MW/m}^2$  design of Table 5.3.-II.

acceptable plant factor because of the constant time assumed for each FPC replacement.

The RFP reactor has been examined over a range of neutron wall loadings and varying utilization of resistive versus superconducting magnets. Recent emphasis has been placed on compact, resistive-coil approaches because of the promise of substantial economic, operational, and development advantages for these physically smaller systems. These improved fusion reactors have an FPC power density in the range 5-15 MWt/m<sup>3</sup> and a mass power density in the range 500-1000 kWe/tonne, which represent improvements by factors of 10-30 compared with earlier fusion reactor designs. Because the cost of FPC is a smaller portion of the total plant cost (typically 7% compared with 25-30% for earlier designs), the unit direct cost, UDC(\$/kWe), is less sensitive to related physics and technology uncertainties; installation and maintenance requirements are also eased. A faster, less costly development path also becomes a possibility. Both physics and technological problems remain to be solved for these higher power-density systems, however. The Strawman designs and the relative sensitivities presented in the following subsection serve as a basis for quantitative assessment of the above-described issues.

### 5.3.2. "Strawman" Design-Point Selection

Although the sensitivity/trade-off studies reported in the previous subsection were performed at a conservative baseline of  $\beta_{\Theta} = 0.13$ , the TITAN Physics Advisory Committee has since recommended a value closer to 0.20, consistent with the best presently-available experimental values. Figure 5.3.-5 presents the COE as a function of  $r_p$  for  $\beta_h = 0.20$ ,  $A \equiv R_T/r_p = 6.5$ , and for various values of power output  $P_E$  in the range 400-1,200 MWe(net). Contours of constant 14.1-MeV-neutron first-wall loading are also shown, together with contours of constant  $\nu$ , the  $\tau_E(\text{PHYS})$  scaling exponent, corresponding to  $\tau_E(\text{OPT}) = \tau_E(\text{PHYS})$ .

Consistent with Fig. 5.3.-5, new Strawman design points have been generated, incorporating the following features:

1.  $\beta_{\Theta} = 0.20$  at  $\Theta = 1.53$  and  $F = -0.10$ .
2. OFCD Q-values,  $Q_p = 535$  and  $Q_c = 9969$  (see Sec. 4.6).
3. Operation at a higher average plasma temperature  $T = 20$  keV to reduce reactive-power dissipation in the shell and other structures during OFCD. Costs ( $\approx 35$  mills/kWeh at  $I_w \approx 18$  MW/m<sup>2</sup>) are insensitive to  $T$  in the range 10-20 keV.

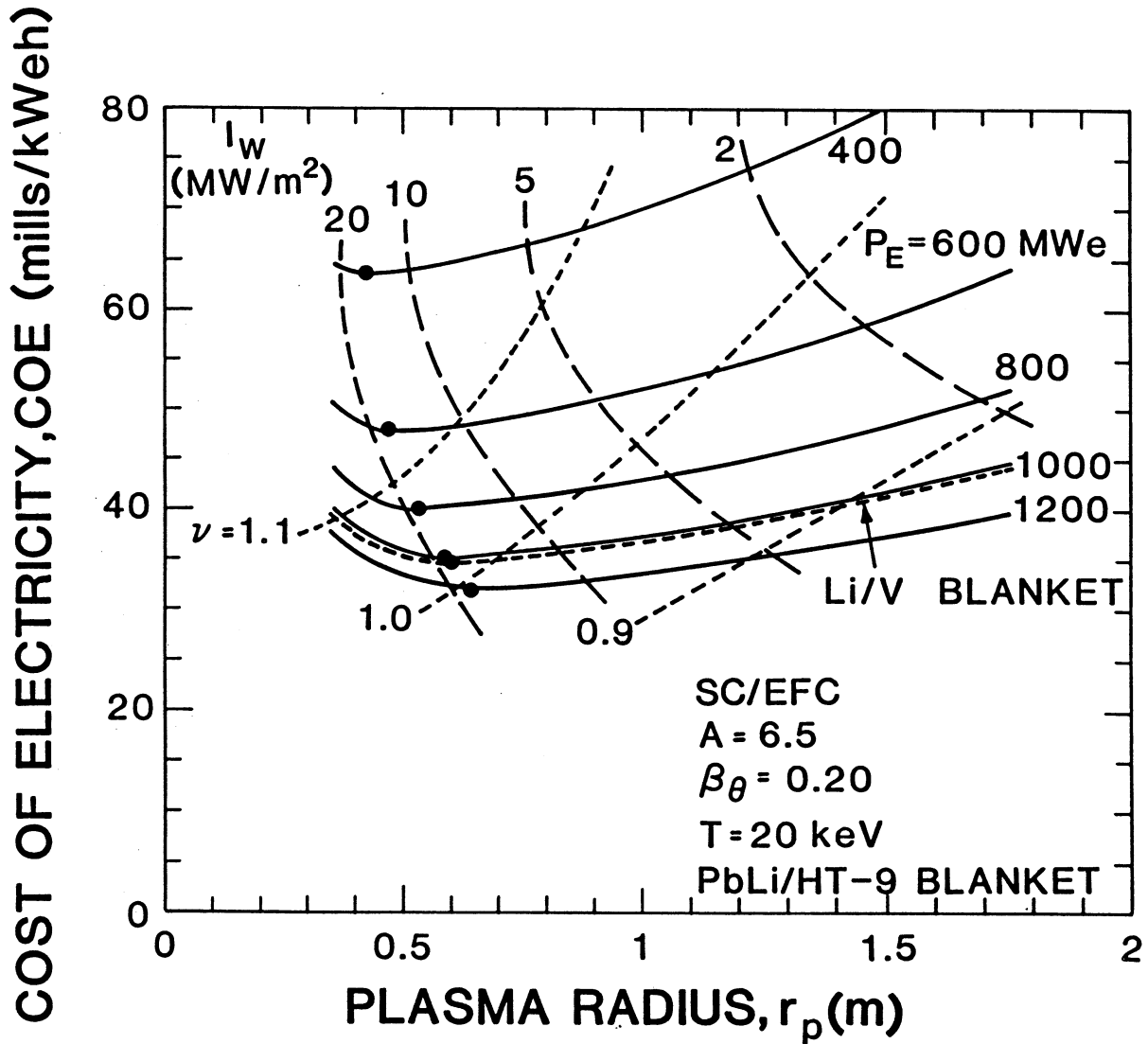


Fig. 5.3.-5. The Cost of electricity, COE, for a compact RFP reactor with PbLi/HT-9 blanket as a function of plasma radius,  $r_p$ , for a range of  $P_E$  values. The COE of a 1000 MWe RFP reactor with Li/V blanket is also shown. Contours of constant  $I_w$  as well as the condition where  $\tau_E(OPT) = \tau_E(PHYS)$  are shown assuming  $\tau_E(PHYS) \propto I_w^\nu r_p^2 f(\beta_\theta)$  scaling and a range of  $\nu$  values.

4. Superconducting EFCs (SC/EFC). The COE for a normal-conducting-EFC (NC/EFC) case at a neutron wall loading  $I_w \approx 18 \text{ MW/m}^2$  is  $\sim 37$  mills/kWeh, equal to about that for the  $\beta_0 = 0.13$  SC/EFC min-COE Strawman.
5. Stray vertical magnetic fields are below target levels (2.5 mT).

The minimum-COE design point at 1,000 MWe(net) has a plasma radius  $r_p = 0.605 \text{ m}$  and  $I_w \approx 18 \text{ MW/m}^2$ . For the convenience of the mechanical engineers, plasma and wall radii  $r_p = 0.60 \text{ m}$  and  $r_w = 0.65 \text{ m}$ , respectively, are specified, at which  $I_w = 18.1 \text{ MW/m}^2$ . Previously, the plasma radii for the  $I_w = 10$  and  $5 \text{ MW/m}^2$  Strawman were  $r_p = 0.85$  and  $1.20 \text{ m}$ , respectively. These Strawman design points are illustrated in Fig. 5.3.-6. Retaining these dimensions for convenience, the corresponding neutron wall loadings now become 9.3 and  $4.8 \text{ MW/m}^2$ . The dimensions of these Strawman designs are summarized in Table 5.3.-III, including parameters for a new  $I_w = 15.6 \text{ MW/m}^2$  case. The schematic geometry was illustrated in Fig. 5.3.-1, which defines the geometric parameters. A more detailed parameter summary of the Strawman, updating Table 5.3.-IV of Ref. 31, is presented in Table 5.3.-IV.

The  $I_w \approx 19 \text{ MW/m}^2$  (min-COE) Strawman design was subjected to PF coil set discretization using the CCOIL magnetics code. This design is illustrated in Fig. 5.3.-7. The PFC position and currents are summarized in Table 5.3.-V. Table 5.3.-VI compares coil performance parameters as obtained from the RFP9 systems code (LA-CC-86-4) and the CCOIL code (Sec. 4.4.2). Circuit parameter from the two codes are compared in Table 5.3.-VII. These parameters are used as input to the CRFPR time-dependent start-up code (LA-CC-86-6), which is being used to optimize the start-up transient (Sec. 4.5.2). Modeling of the early-time RFP formation phase is also under investigation (Sec. 4.5.1).

### 5.3.3. Alternative Configuration Options

Modification to the RFP9 parametric systems analysis (PSA) code to model alternative configuration options, including the integrated blanket coil (IBC) and water (pool) configuration are under development. Characterization of these options is less well-developed than are the models of the more conventional liquid-metal-loop configuration.

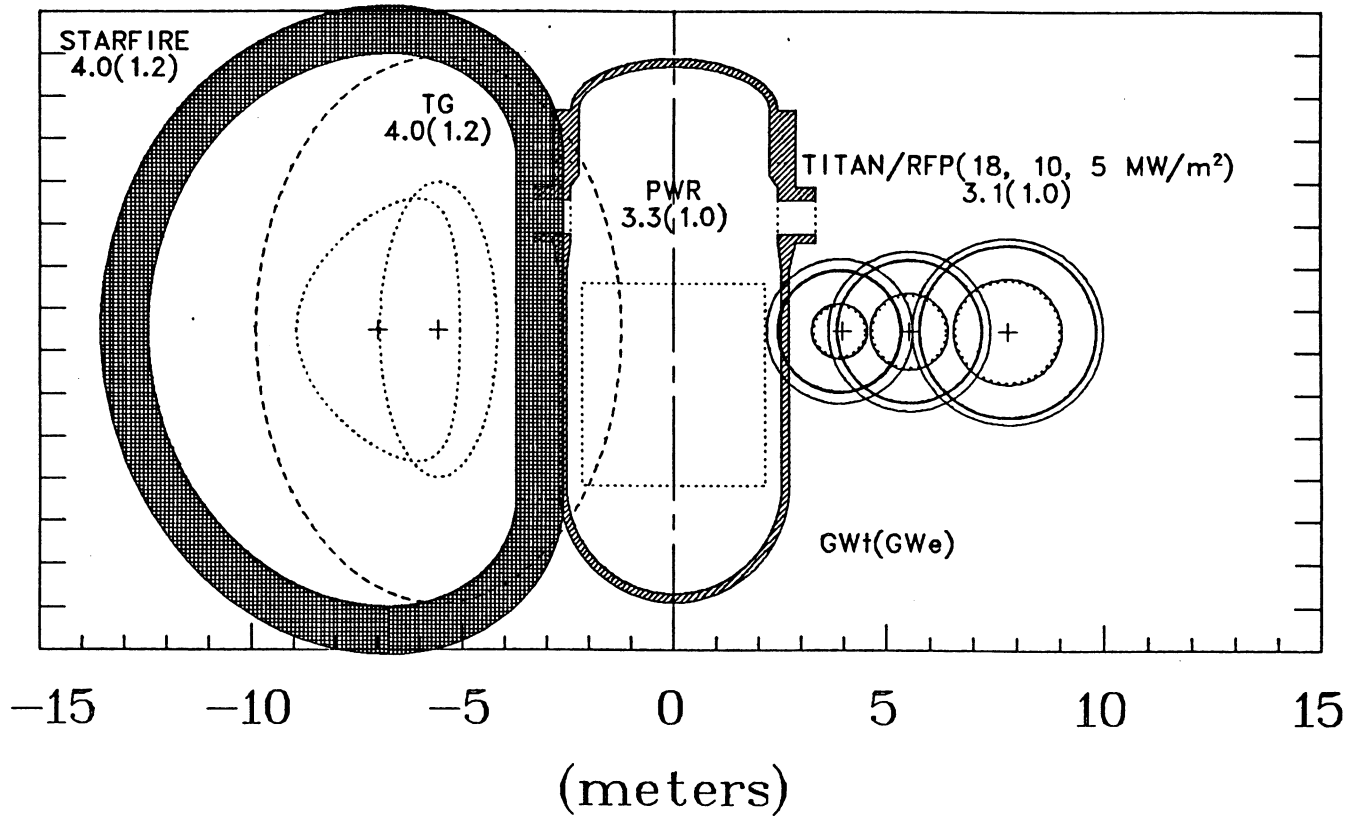


Fig. 5.3.-6. Elevation views of three TITAN Strawman design points compared with a fission PWR [36], the STARFIRE tokamak design [17], and the GENEROMAK tokamak design [16]. The TITAN coil set are not shown in discretized form.

TABLE 5.3.-III

TITAN STRAWMAN<sup>(a)</sup> DIMENSIONS (m)  
 (Refer to Fig. 5.3.-1 for dimension definition)

$I_w$ (MW/m <sup>2</sup> )	18.1 <sup>(b)</sup>	15.6	9.3	4.8
$R_T$	3.90	4.225	5.525	7.80
$r_p$	0.60	0.65	0.85	1.20
$r_w$	0.65	0.70	0.90	1.25
$r_{bo}$ <sup>(c)</sup>	1.425	1.475	1.675	2.025
$r_{TFo}$ <sup>(d)</sup>	1.453	1.501	1.695	2.041
$r_{PFO}$ <sup>(e)</sup>	1.705	1.735	1.883	2.199
$R_{EF}$	6.244	6.605	8.069	10.67
$z_{EF}$	2.726	2.771	2.971	3.358
$\delta_{EF}$ <sup>(f)</sup>	0.697	0.680	0.634	0.594

(a) SC/EFC,  $\beta_\Theta = 0.20$ ,  $A = R_T/r_p = 6.5$ ,  $P_E = 1000$  MWe(net).

(b) Minimum-COE.

(c)  $\Delta b = 0.775$  including first wall, blanket, and shield.  $r_{bo} = r_w + \Delta b$ .

(d)  $r_{TFo} = r_{TF} + \delta_{TF}/2$ .

(e)  $r_{PFO} = r_{PF} + \delta_{PF}/2$ .

(f)  $\Delta s_{EF} = 0.5$  m.

TABLE 5.3.-IV  
SUMMARY OF 1000-MWe(net) TITAN STRAWMAN  
FOR THREE NEUTRON WALL LOADINGS<sup>(a)</sup>

Neutron Wall Loading, $I_w$ (MW/m <sup>2</sup> )	18.1	9.3	4.8
<u>Plasma Parameters</u>			
Minor plasma radius, $r_p$ (m)	0.60	0.85	1.20
Major plasma radius, $R_T$ (m)	3.90	5.525	7.80
Plasma volume, $V_p$ (m <sup>3</sup> )	27.7	78.8	221.7
Plasma current, $I_\phi$ (MA)	17.75	19.40	21.19
Toroidal current density, $j_\phi$ (MA/m <sup>2</sup> )	15.7	8.5	4.7
Plasma density, $n$ (10 <sup>20</sup> /m <sup>3</sup> )	4.35	2.59	1.55
Energy confinement time, $\tau_E$ (s)	0.25	0.42	0.71
Thermal diffusivity, $\chi_E$ (m <sup>2</sup> /s)	0.27	0.32	0.38
Fusion power density, $P_F/V_p$ (MW/m <sup>3</sup> )	81.6	28.9	10.4
Plasma ohmic dissipation, $P_\Omega$ (MW)	8.0	6.8	5.8
<u>Poloidal-Field Quantities</u>			
Coil thickness, $\delta_{c\theta}$ (m)	0.252	0.188	0.158
Average minor radius, $r_{c\theta}$ (m)	1.579	1.789	2.120
Poloidal field at plasma surface, $B_\theta$ (T)	5.92	4.56	3.35
Coil field, $B_{c\theta}$ (T)	2.25	2.17	2.00
OHC current density, $j_{c\theta}$ (MA/m <sup>2</sup> )(b)	17.4	16.9	15.5
Mass of coil, $M_{OHC}$ (tonnes)	322.3	386.0	543.1
EFC current density, $j_{c\theta}$ (MA/m <sup>2</sup> )(c)	19.8	21.2	22.2
Mass of coil, $M_{EFC}$ (tonnes)	278.5	297.1	344.9
Poloidal-field stored energy, $W_{B\theta}$ (GJ)	4.6	5.2	6.4
OHC dissipation during back-bias (MW)	285.0	342.0	422.0
<u>Toroidal-Field Quantities</u>			
Coil thickness, $\delta_{c\phi}$ (m)	0.028	0.020	0.016
Average minor radius of coil, $r_{c\phi}$ (m)	1.439	1.685	2.033
Mass of coil, $M_{TFC}$ (tonnes)	28.5	37.7	54.1
Reversed-toroidal field during burn, $-B_{\phi R}$ (T)	0.36	0.28	0.22
Magnetic energy stored in coil, $W_{B\phi}$ (GJ)	0.78	0.96	1.22
TFC current density, $j_{c\phi}$ (MA/m <sup>2</sup> )	17.4	16.9	15.5
Ohmic dissipation during burn, $P_\Omega^{TFC}$ (MW)	34.0	42.1	51.0
Mass of divertor coil, $M_{DFC}$ (tonnes)	3.8	3.9	4.1
Ohmic dissipation in divertor, $P_\Omega^{DFC}$ (MW)	23.7	24.4	25.6

TABLE 5.3.-IV (cont)

<u>Engineering Summary</u>			
Engineering Q-value, $Q_E = 1/\epsilon$	7.84	7.47	7.09
Fusion power, $P_F$ (MW)	2,261.0	2,279.0	2,298.0
Total thermal power, $P_{TH}$ (MW)	2,866.0	2,886.0	2,910.0
First-wall minor radius, $r_w$ (m)	0.65	0.90	1.25
FPC minor radius, $r_s$ (m)	1.71	1.88	2.20
Masses (tonnes)			
♦ first wall/blanket	39.7	66.4	116.0
♦ shield	875.2	1,119.0	1,513.8
♦ total coil set	633.1	724.8	946.2
♦ FPC (FW/B/S/C) <sup>(d)</sup>	1,553.2	1,919.8	2,595.8
♦ FPC structure	663.5	912.9	1,317.5
System power density, $P_{TH}/V_{FPC}$ (MWt/m <sup>3</sup> )	12.8	7.5	3.9
Mass power density, $1000P_E/M_{FPC} = MPD$ (kWe/tonne) <sup>(d)</sup>	644.0	521.0	385.0
<u>Cost Summary</u>			
Cost of electricity, COE(mills/kWeh)	35.2 <sup>(e)</sup>	36.5	39.0
Unit direct cost, UDC(\$/kWe)	1,409.0	1,463.0	1,569.0
Total cost, TC(M\$)	1,920.0	1,993.0	2,139.0
FPC unit cost (\$/kg) <sup>(e)</sup>	52.0	53.0	55.0
Fractions of total direct cost (TDC)			
♦ reactor plant equipment, RPE/TDC	0.35	0.37	0.41
♦ fusion power core cost, FPC/TDC <sup>(d)</sup>	0.057	0.069	0.091

(a) All designs for baseline parameters:  $T = 20$  keV,  $A = 6.5$ ,  $\beta_\theta = 0.20$ ,  $\eta_{TH} = 0.40$ .

(b) Peak current in back-biased state, decreases by factor of  $\sim 2$  in forward-bias state, subsequently decays to zero upon initiation of OFCD.

(c) Superconducting magnet.

(d) Does not include structure.

(e) Minimum COE.

TABLE 5.3.-V  
PF COIL LOCATIONS AND PARAMETERS

	R(m)	$\pm z$ (m)	$\Delta R$ (m)	$\Delta z$ (m)	A(m <sup>2</sup> )	j(MA/m <sup>2</sup> )	I(MA)
EFC	6.4959	2.4873	0.6973	0.6973	0.4862	18.2675	8.8821
OHC-1	5.8699	1.9473	0.4000	0.4000	0.1600	12.8372	-2.0540
2	3.9472	2.2299	0.4100	0.4100	0.1681	12.2187	-2.0540
3	3.1958	1.8533	0.3000	0.5000	0.1500	13.6930	-2.0540
4	2.7905	1.4625	0.2000	0.5000	0.1000	20.5396	-2.0540
5	2.5503	1.1031	0.2500	0.3300	0.0825	24.8965	-2.0540
6	2.4028	0.7705	0.3300	0.3000	0.0990	20.7470	-2.0540
7	2.3163	0.4557	0.3200	0.3000	0.0960	21.3954	-2.0540
8	2.2759	0.1508	0.3300	0.3000	0.0990	20.7470	-2.0540

TABLE 5.3.-VI  
COMPARISON OF COIL PARAMETERS

<u>Parameter</u>	<u>Systems Code</u>	<u>CCOIL</u>
EFC current (MA) <sup>(a)</sup>	19.2	17.8
EFC volume (m <sup>3</sup> )	38.1	39.7
EFC mass (tonne)	278.3	292.1
EFC Joule losses (MW) <sup>(a)</sup>	0.0	(378.0 NC)(0.0 SC)
EFC peak field (T) <sup>(a)</sup>	10.2	5.9
EFC current density (MA/m <sup>2</sup> ) <sup>(a)</sup>	19.8	18.3
OHC current (MA)		
♦ back bias	-31.4	-32.9
♦ forward bias	17.6	15.1
OHC volume	43.7	40.9
OHC mass (kg)	318.9	301.2
OHC Joule losses (MW)	0.0/287.1	(68. <sup>(c)</sup> )/321. <sup>(b)</sup>
OHC Von Mises stress (MPa) <sup>(b)</sup>	186.	215.6
OHC peak field (T) <sup>(b)</sup>	--	8.3
OHC current density (MA/m <sup>2</sup> ) <sup>(b)</sup>	7.9/17.6	(12.2-24.9)
OHC stray vertical field (mT) <sup>(b)</sup>	--	1.25(< 2.45)
PFC transparency (%)	--	67.2
TFC transparency (%)	--	TBD

(a) Steady-state values.

(b) Back-bias values.

(c) Forward-bias values.

TABLE 5.3.-VII  
COMPARISON OF PF CIRCUIT PARAMETERS

<u>Parameter</u>	<u>Systems Code</u>	<u>CCOIL</u>
Self-Inductances ( $\mu\text{H}$ )		
♦ $L_p$	13.24	13.24
♦ $L_{EF}$	25.22	14.8
♦ $L_{OH}$	3.61	3.4
Mutual Inductances ( $\mu\text{H}$ )		
♦ $M_{OH,p}$	3.61	3.47
♦ $M_{OH,EF}$	--	3.08
♦ $M_{EF,p}$	3.70	3.87
Current Levels (MA)		
♦ $I_\phi$	17.75	17.75
♦ $I_{EF}$	19.22	17.8
♦ $\Delta I_{OH}$	45.42	48.0
Magnetic Fluxes (Wb)		
♦ Plasma	235.0	235.0
♦ EFC	71.1	68.8
♦ OHC	163.9	166.0

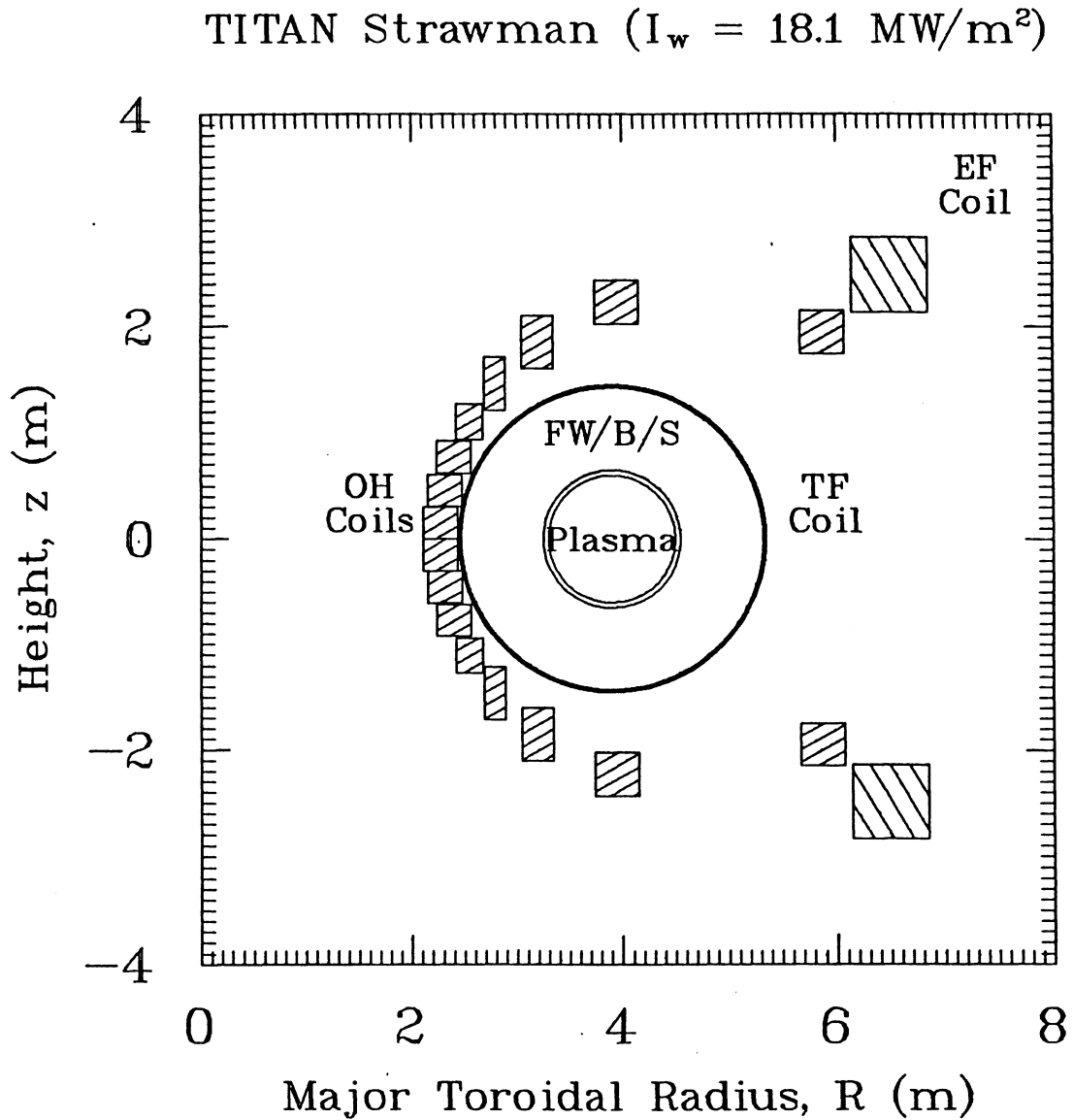


Fig. 5.3.-7. Elevation view of the  $I_w \approx 18 \text{ MW/m}^2$  (min-COE) TITAN Strawman design point with the PF coil set determined by the CCOIL code. The EFCs are superconducting.

REFERENCES

1. R. L. Hagenon and R. A. Krakowski, "Compact Reversed-Field Pinch Reactors (CRFPR): Sensitivity Study and Design-Point Determination," Los Alamos National Laboratory Report LA-9389-MS (July 1982).
2. R. L. Hagenon, R. A. Krakowski, C. G. Bathke, R. L. Miller, M. J. Embrechts, N. M. Schnurr, et al., "Compact Reversed-Field Pinch Reactors (CRFPR): Preliminary Engineering Considerations," Los Alamos National Laboratory Report LA-10200-MS (August 1984).
3. C. Copenhaver, R. A. Krakowski, N. M. Schnurr, R. L. Miller, C. G. Bathke, R. L. Hagenon, et al., "Compact Reversed-Field Pinch Reactors (CRFPR): Fusion-Power-Core Integration Study," Los Alamos National Laboratory Report LA-10500-MS (August 1985).
4. R. L. Miller, R. A. Krakowski, C. G. Bathke, C. Copenhaver, N. M. Schnurr, A. G. Englehardt, T. J. Seed, and R. M. Zubrin, "Advanced Tokamak Reactors Based on the Spherical Torus (ATR/ST): Preliminary Design Considerations," Los Alamos National Laboratory Report LA-10740-MS (June 1986).
5. J. D. Callen and R. A. Dory, "Magnetohydrodynamic Equilibria in Sharply Curved Axisymmetric Devices," Phys. Fluids 15 (1972) 1523.
6. D. J. Strickler, J. B. Miller, K. E. Rothe, and Y-K. M. Peng, "Equilibrium Modeling of the TFCX Poloidal Field Coil System," Oak Ridge National Laboratory Report ORNL/FEDC-83/10 (April 1984).
7. H. M. Attaya and M. E. Sawan, "NEWLIT-A General Code for Neutron Wall Loading Distribution in Toroidal Reactors," Fusion Tech. 8 (1985) 609.
8. R. D. O'Dell, F. W. Brinkley, Jr., and D. R. Marr, "User's Manual for ONEDANT: A Code Package for One-Dimensional Diffusion-Accelerated Neutral-Particle Transport," Los Alamos National Laboratory Report LA-9184-M (February 1982).

9. T. J. Seed, "TRIDENT-CTR User's Manual," Los Alamos Scientific Laboratory Report LA-7835-M (May 1979).
10. Los Alamos Monte Carlo Group, "MCNP - a General Monte Carlo Code for Neutron and Photon Transport, Version 3A," Los Alamos National Laboratory Report LA-7396-M, Revised (April 1981).
11. R. L. Miller, C. G. Bathke, R. A. Krakowski, F. M. Heck, L. Green, J. S. Karbowski, et al., "The Modular Stellarator Reactor: A Fusion Power Plant," Los Alamos National Laboratory Report LA-9737-MS (July 1983).
12. P. J. Harbour and J. G. Morgan, "Models and Codes for the Plasma Edge Region," UKAEA Culham Laboratory Report CLM-R234 (December 1982).
13. N. Jarmie, R. E. Brown, and R. A. Hardenkopf, "Fusion-energy Reaction  ${}^2\text{H}(t,\alpha)n$  from  $E_t = 12.5$  to 117 keV," Phys. Rev. C 29 (1984) 2031 and relevant Erratum in Phys. Rev. C 33 (1986) 385.
14. J. B. Taylor, "Relaxation of Toroidal Plasma and Generation of Reversed Magnetic Fields," Phys. Rev. Lett. 33 (1979) 1139.
15. J. Kessner and R. W. Conn, "Space-Dependent Effects on the Lawson and Ignition Conditions and Thermal Equilibria in Tokamaks," Nucl. Fusion 16 (1976) 397.
16. J. Sheffield, R. A. Dory, S. M. Cohn, J. G. Delene, L. Parsly, D. E. T. F. Ashby, and W. T. Reiersen, "Cost Assessment of a Generic Magnetic Fusion Reactor," Fusion Tech. 9 (1986) 199.
17. C. C. Baker, M. A. Abdou, R. M. Arons, A. E. Bolon, C. D. Boley, J. N. Brooks, et al., "STARFIRE - A Commercial Tokamak Fusion Power Plant Study," Argonne National Laboratory Report ANL/FPP-80-1 (September 1980).
18. B. G. Logan, C. D. Henning, G. A. Carlson, R. W. Werner, D. E. Baldwin, W. L. Barr, et al., "MARS Mirror Advanced Reactor Study Final Report," Lawrence Livermore National Laboratory Report UCRL-53480 (July 1984).

19. S. C. Schulte, T. L. Wilke, and J. R. Young, "Fusion Reactor Design Studies--Standard Accounts for Cost Estimates," Battelle (Pacific Northwest Laboratory) Report PNL-2648 (May 1978).
20. S. C. Schulte, W. E. Bickford, C. E. Willingham, S. K. Ghose, and M. G. Walker, "Fusion Reactor Design Studies-Standard Cost Estimating Rules," Battelle (Pacific Northwest Laboratory) Report PNL-2987 (May 1979).
21. W. R. Hamilton, D. C. Keeton, and S. L. Thomson, "Cost Accounting System for Fusion Studies," Oak Ridge National Laboratory Report ORNL/FEDC-85/7 (December 1985).
22. S. L. Thomson, "Reference Cost Data for Fusion," Oak Ridge National Laboratory Report ORNL/FEDC-86/8 (to be published, 1986).
23. R. A. Krakowski, R. L. Hagenson, N. M. Schnurr, C. Copenhaver, C. G. Bathke, and R. L. Miller, "Fusion-Power-Core Integration Study for the Compact Reversed-Field Pinch Reactor (CRFPR): A Follow-On Study," Nucl. Eng. and Design 4 1986 75 (also LA-UR-85-3614).
24. R. A. Krakowski, R. L. Miller, C. G. Bathke, R. L. Hagenson, "Compact Reversed-Field Pinch Reactors (CRFPR)," IAEA Technical Committee Meeting and Workshop on Fusion Reactor Design and Technology, Yalta, USSR (May 29 - June 6, 1986) (also LA-UR-86-1229).
25. M. K. Bevir and J. W. Gray, "Relaxation, Flux Consumption and Quasi Steady State Pinches," Proc. RFP Theory Workshop, Los Alamos, NM (April 28 - May 2, 1980), Los Alamos National Laboratory Report LA-8944-C (January 1982) 176.
26. K. F. Schoenberg, R. F. Gribble, and D. A. Baker, "Oscillating Field Current Drive for Reversed Field Pinch Discharges," J. Appl. Phys. 56 (1984) 2519.
27. C. G. Bathke, R. A. Krakowski, and R. L. Miller, "A Comparison Study of Toroidal-Field and Bundle Divertors for a Compact Reversed-Field Pinch Reactor," Fusion Technol. 8 (1985) 1616.

28. R. A. Krakowski, R. L. Miller, and J. G. Delene, "Directions for Improved Fusion Reactors," IAEA Technical Committee Meeting and Workshop on Fusion Reactor Design and Technology, Yalta, USSR (May 29 - June 6, 1986) (also LA-UR-86-1386).
29. R. A. Krakowski, R. L. Miller, and R. L. Hagenson, "Prospects for Improved Fusion Reactors," Fourth European Nuclear Conference (ENC-86), (June 1 - 6, 1986). Also LA-UR-86-641.
30. H. A. B. Bodin, R. A. Krakowski, and S. Ortolani, "The Reversed-Field Pinch: From Experiment to Reactor," Fusion Tech. 10 (1986) 307.
31. R. L. Miller, R. A. Krakowski, C. G. Bathke, K. A. Werley, and R. L. Hagenson, "Fusion Reactor Options and Alternatives for the RFP," Seventh ANS Topical Meeting on the Tech. of Fusion Energy, Reno, NV (June 15 - 19, 1986), Fusion Tech. 10 (1986) 1159. Also LA-UR-86-1864 (Rev.).
32. Y-K. M. Peng, et al., "Spherical Torus: An Approach to Compact Fusion at Low Field-Initial Ignition Assessment," Fusion Tech. 8 (1985) 338.
33. United Engineers and Constructors, Inc., "1000-MWe Central Station Power Plants Investment Cost Study," U. S. A. E. C. Report WASH-1230 (June 1972).
34. B. D. Trauger (ed.), "Nuclear Options Viability Study: Volume III, Nuclear Discipline Topics," Oak Ridge National Laboratory Report ORNL/TM-9780/3 (May 1986).
35. J. H. Crowley and R. E. Allan, "Phase VII Update (1984) Report for the Energy Economic Data Base Program: EEDB-VII," Department of Energy Report DOE/NE-0051/2 (August 1985).
36. A. Walker, "Design of the PWR for Sizewell 'B'," The Nuclear Engineer 24 (1984) 176. Also, UK Central Electricity Generating Board Brochure, "A Technical Outline of Sizewell 'B' The British Pressurized Water Reactor," (1983).